

Non-silica microstructured optical fibers for mid-IR supercontinuum generation from 2 μm – 5 μm

Jonathan H.V. Price^{*}, Tanya M. Monro², Heike Ebendorff-Heidepriem², Francesco Poletti¹, Vittoria Finazzi, Julie Y.Y. Leong¹, Periklis Petropoulos¹, Joanne C. Flanagan[†], Gilberto Brambilla¹, Xian Feng¹, David J. Richardson¹

¹ Optoelectronics Research Centre, University of Southampton, SO17 1BJ, UK

² currently with The School of Chemistry and Physics, University of Adelaide, Australia

ABSTRACT

We have performed numerical simulations to investigate the optimization of compound glass microstructured optical fibers for mid IR supercontinuum generation beyond the low loss transmission window of silica, using pump wavelengths in the range 1.55-2.25 μm . Large mode area fibers for high powers, and small core fiber designs for low powers, are proposed for a variety of glasses. Modeling results showed that for Bismuth and lead oxide glasses, which have nonlinearities ~ 10 x that of silica, matching the dispersion profile to the pump wavelength is essential. For chalcogenide glasses, which have much higher nonlinearities, the dispersion profile is less important. The pump pulses have duration of < 1 ps, and energy < 30 nJ. The fiber lengths required for generating continuum were < 40 mm, so the losses of the fibers were not a limiting factor. Compared to planar rib-waveguides or fiber-tapers, microstructured fiber technology has the advantages of greater flexibility for tailoring the dispersion profile over a broad wavelength span, and a much wider possible range of device lengths.

Keywords: Nonlinear optics, fibers, materials; supercontinuum; tapers, infrared, microstructured.

1. INTRODUCTION

Since microstructured optical fibers (MOF) first enabled visible supercontinuum generation using seed pulses directly from a Ti:sapphire oscillator¹, there has been tremendous interest to explain this remarkable spectral broadening^{2,3} and to develop further applications of these fibers⁴. The use of MOF for supercontinuum generation is particularly attractive since small core sizes can be realized, increasing fiber nonlinearity, and because the zero dispersion wavelength (ZDW) can be tailored to maximize supercontinuum generation for a given pump wavelength. In the visible and near IR, applications for these sources include optical frequency metrology⁵ and optical tomography⁶. Other applications for broadband continuum exist for wavelengths beyond 2 μm , for example LIDAR applications in the 3-12 μm wavelength range.

Beyond a wavelength of 2 μm , limited by the transparency of silica, it is necessary to consider alternative glasses for generation of broadband radiation. The fundamental material properties of non-silica “compound” glasses can enhance supercontinuum generation across the mid-IR. The zero-dispersion wavelength of the material is strongly dependent on the choice of glass, and one particularly attractive option is to shift the fiber zero-dispersion to below 2 μm to offer the potential to use diode pumped solid state lasers operating at 2 μm to generate the supercontinuum. Seeding at 1.55 μm from an Er-fiber pump system is a very attractive option and seed wavelengths of 2.0-2.25 μm are also readily accessible from commercially available optical parametric oscillator and amplifier (OPO/OPA) systems.

Compound glasses have not yet found widespread application due to the difficulty in fabricating low-loss single mode fibers. However, microstructured fiber technology provides a powerful new technique for producing compound glass structures. Recent work at the University of Southampton has led to successful fabrication of the first compound glass microstructured fibers. Investigations of the fibers’ non-linear and dispersive properties will help establish their suitability, or otherwise, as a temporally agile, frequency selective sources. For example, a compound glass microstructured fiber with $\gamma = 1860 / (\text{W.km})$ was reported recently⁷.

^{*} jhvp@orc.soton.ac.uk

[†] Please note that Joanne C. Flanagan has previously published under the name of Joanne C. Baggett

For many applications a small fiber core is a desirable feature since it greatly relaxes the source power requirements, however for others where it is necessary to generate high average signal powers this can be a disadvantage as it ultimately limits the pulse energies that can be used. With a limit on the maximum pulse energy, the only way to produce high average power is to vastly increase the repetition rate of the laser and in order to increase the pulse energy requirement to satisfy average power needs for reasonable pulse repetition rates it becomes necessary to work with fibers with a larger core area. In this instance the dispersion of the fiber is dominated by the material dispersion. Consequently one can envisage a need for two sorts of fiber and two sorts of pump laser suited for either high or low power applications.

In this paper we present the results of numerical simulations which show the optimum glass-type and fiber-design combinations for mid-IR supercontinuum generation when pumped at near-IR wavelengths. To generate the required nonlinear response, we have considered sub-picosecond pumping using a seed wavelength close to the fiber zero dispersion wavelength (ZDW), which is the usual configuration for demonstrations of visible supercontinuum generation using Ti:Sapphire¹ or rare-earth doped fiber pump lasers^{8,9}.

Using numerical simulations to predict the supercontinuum spectra, we take small core Bi MOF as a reference, with the seed pulse wavelength equal to the fiber ZDW, and investigate the influence of seed pulse energy and duration, and of dispersion, nonlinearity and loss, by changing each parameter in isolation. Then to consider an example of a real glass with much higher intrinsic nonlinearity, we performed additional simulations for a small core GLSO MOF, again with the seed pulse wavelength equal to the fiber ZDW. We then performed simulations for large mode fibers which have drastically changed properties compared to small core fibers because the dispersion of large mode fibers is dominated by the material, and is not a variable. We then discuss our conclusions.

We expect that our mid-IR simulations, although not an exact prediction, should provide a reasonable guide to the spectra that might be possible from future experimental work. Our numerical model is similar to that used by other authors for studying visible continuum in silica MOF^{10,11}. In addition, we have previously published a study of visible/UV supercontinuum generation from a silica MOF¹² and a study of visible/NIR supercontinuum from an extruded SF57 MOF¹³. Both of these studies combined experimental and numerical results, and the simulations and experiments were in qualitative agreement.

This paper is structured as follows. Section 2 presents an overview of the multicomponent glass properties and waveguide fabrication technologies. Section 3 presents fiber designs that use the selected glass types and that achieve a ZDW close to the chosen pump wavelengths. Section 4 presents modeling predictions for the supercontinuum spectra. Section 5 contains our conclusions and our suggestions about desirable fiber properties for future investigation.

2. GLASS CHOICE AND FABRICATION TECHNOLOGIES

Supercontinuum generation at mid-IR wavelengths requires the use of a highly nonlinear optical medium with high mid-IR transparency. Extending current MOF technology developed from silica based work at visible and near-IR wavelength ($\sim 0.4 - 1.7 \mu\text{m}$) to mid-IR wavelengths ($> 2 \mu\text{m}$) necessitates developing a detailed understanding of the relationship between the glass composition and the optical properties, such as the position of the multiphonon absorption edge and nonlinear refractive index, etc, in order to select a suitable glass for the fibers. In addition to the material considerations, we also consider multiple fabrication approaches in order to tailor the dispersion and nonlinearity of the fibers.

The absorption of a solid in the long wavelength limit is known as the multiphonon or IR absorption edge and arises from inner molecule or lattice vibrations. A simple Hooke's law mass on spring model predicts that the multiphonon absorption edge will shift towards longer wavelengths if heavier atoms are introduced into the glass network or if chemical bonds are weakened. The multiphonon absorption edges of several glasses are shown in Fig. 1 (a)¹⁴. Note that due to the strong Si-O bonding, the oxide containing SiO₂ cannot be transparent at the wavelengths longer than $5 \mu\text{m}$, whilst glasses containing any oxide cannot be transparent at the wavelengths longer than $\sim 8 \mu\text{m}$. We reviewed data on a variety of glass compositions, and selected those with transmission loss due to multiphonon absorption of less than 2 dB/m at $2 \mu\text{m}$ for further consideration.

In addition to the phonon losses, extrinsic losses due to scattering and impurity absorption affect the glass transmission below the intrinsic maximum transmission wavelength. Oxide glasses readily incorporate OH impurities, which can result in losses of more than 1000 dB/m at certain wavelengths as shown in Fig. 1. (b). Dehydration techniques such as addition of fluoride and dry/reactive gas treatment can decrease the OH loss substantially. Fluoride glasses are generally

less susceptible to OH impurities, and dehydration can then decrease the OH loss to as low as 0.001 dB/m¹⁵. In oxide glasses, the OH bands are very broad ranging over the whole mid-IR range, whereas the OH band of fluoride and chalcogenide glasses is confined to 2.8-3.4 μm . The OH and SH contents of chalcogenide glasses depend on the melting conditions and with careful environmental control during fabrication, GLS glass can be produced with low OH absorption of 8 dB/m at 3 μm as shown in Fig. 1. (b). Commercial As₂S₃ fibers exhibit OH absorption of <2 dB/m at 3 μm and SH absorption of 2-10 dB/m at 4 μm ^{16,17}.

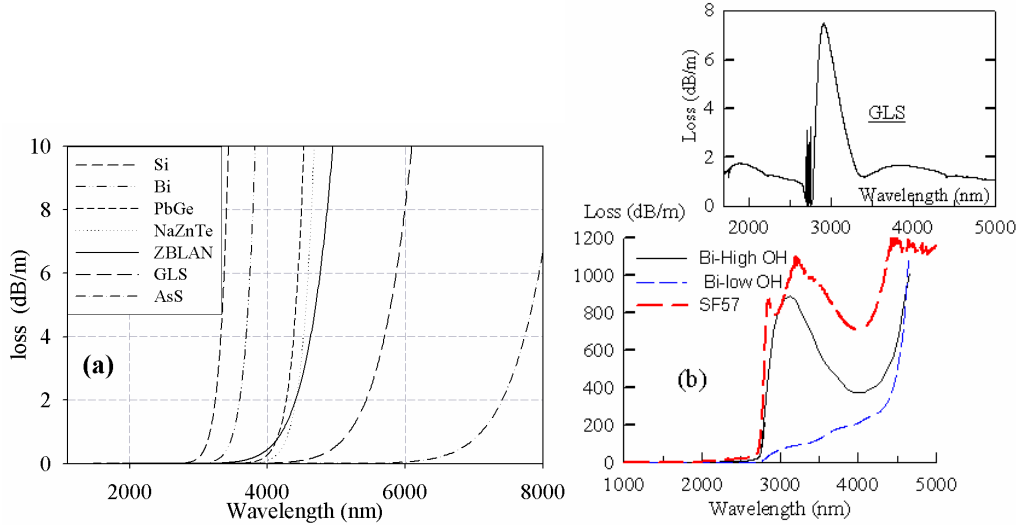


Fig. 1. (a) Multiphonon edge of different glasses. (b) Loss spectra of different glasses (used in simulations) as measured using unclad fiber and cutback technique as well as bulk samples of 1 - 30 mm thickness and commercial spectrometers.

The refractive index, and its variation with wavelength (hence dispersion), are also dependent on glass composition. According to the empirical Miller rule, the third-order nonlinear dielectric susceptibility $\chi^{(3)}$ is proportional to the fourth power of the linear susceptibility $\chi^{(1)}$. A high nonlinear refractive index is expected to be achieved in glasses composed of ions with high polarizability. However, the Miller rule is just an empirical relationship and consequently can only be used as a rough indication of those materials with high values of n_2 and accurate values of n_2 can only be obtained from experiments, which may also have been performed at different wavelengths for different glasses. Fig. 2. shows a summary of the relation between the linear refractive index n and nonlinear refractive index n_2 in various glasses¹⁸. It can be seen that introducing heavy atoms (i.e. heavy metal compounds) or ions with a large ionic radius (i.e. using chalcogen elements S, Se and Te to replace oxygen), which both act to increase the polarizability of the components in the glass matrix, also increases the nonlinear index n_2 .

Although a remarkable degree of dispersion management can be achieved using extremely high mode confinement in MOF structures, for applications such as supercontinuum generation that depend on the dispersion over broad wavelength ranges, dispersion management is a delicate balance between fiber design and material properties and an inherently favourable material dispersion is important. To predict the refractive indices of the glasses at wavelengths above 2 μm we have used the measured refractive index data^{16,19,20} fitted to a generalized Sellmeier equation. We have also calculated the material dispersion, D_{MAT} , for several glasses (Fig. 2. (b)) from the Sellmeier equation fits. The linear and nonlinear indices of different glasses are listed in Table 1. The ZDW of a glass shifts to longer wavelength with increasing linear refractive index. Heavy metal oxide glasses (lead-silicate, bismuth-oxide, tellurite) have linear indices in the range of 1.8-2.0, nonlinear indices that are ~ 10 times higher than silica, material ZDWs of 2-3 μm , and multiphonon absorption edge of ~ 3.5 μm . Chalcogenide glasses (GLS, As₂S₃), linear indices of 2.2-2.4, nonlinear indices significantly greater than those of the oxide glasses, and ZDWs larger than 4 μm .

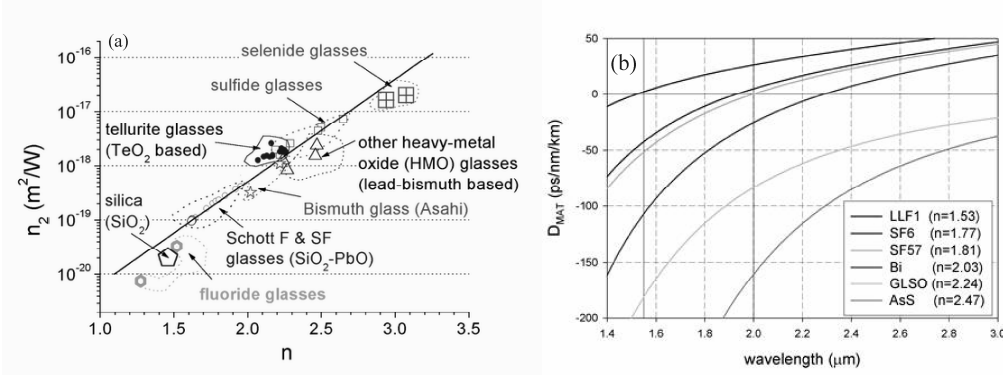


Fig. 2. (a) Relation between the linear refractive index n and nonlinear refractive index n_2 in various glasses. (b) Material dispersion curves of Schott glasses (LLF1,SF6,SF57), chalcogenide glass (GLSO) and bismuth oxide glass (Bi). The numbers in the legend indicate the linear index at 1.06 μm .

Based on the above study, it can be seen that heavy metal oxide and chalcogenide based glasses are promising candidates for developing mid-IR nonlinear MOFs. The chalcogenide glasses possess advantages over the heavy metal oxide glass systems in terms of higher n_2 and longer wavelength multiphonon absorption edges. However, the toxicity, chemical durability and thermal stability of the heavy metal oxide based glasses are typically superior to those of the chalcogenide based glasses. As a brief conclusion for the glass selection, we believe that heavy-metal oxide glasses have adequate properties for achieving mid-IR continuum between 2 – 4 μm , and are technologically the best developed candidates for immediate experiments. Chalcogenide glasses are very promising for a broad range of mid IR applications in the future.

glass type	code	main components	n_0	$n_2 \times 10^{20}$ (m ² /W)	ZDW (μm)
silica	Si	SiO ₂	1.45	2.7 ²¹	1.26 ²²
lead silicate	SF57	PbO-SiO ₂	1.81	41 ²³	2.00
bismuth oxide	Bi	Bi ₂ O ₃	2.02	32 ²⁴	2.29
germanate	PbGe	PbO-GeO ₂	1.80	22 ²⁵	1.78 ^{b22}
tellurite	ZnTe	ZnO-TeO ₂	2.03	51 ^{a 21}	2.24 ^{a22}
fluoride	ZBLAN	ZrF ₄ -BaF ₂	1.50	3.3 ²¹	1.62 ¹⁵
chalcogenide	AsS	As ₂ S ₃	2.44	200 ²⁶	4.81
	GLS	Ga ₂ S ₃ -La ₂ S ₃	2.41	216 ²⁷	
	GLSO	Ga ₂ S ₃ -La ₂ O ₃	2.25	177 ²⁷	4.64

^a value for Na₂O-TeO₂ glass, ^b value for Na₂O-GeO₂ glass

Table 1: Properties of different glasses: linear and nonlinear indices n_0 and n_2 at 1.06 μm (Si, PbSi, PbGe, ZnTe, ZBLAN) and 1.5 μm (Bi, AsS, GLS, GLSO), and zero dispersion wavelength (ZDW).

A brief review of fabrication technology is provided in order to establish an appropriate fiber geometry for the design optimization described in the following section. Three waveguide types can provide tight mode confinement to enable both dispersion management and high effective nonlinearity over extended interaction lengths: rib-waveguides, tapering of fibers, and MOFs. For fibers, and, to a lesser extent, tapers, the combination of loss and nonlinearity leads to scaling of device length to achieve an optimum nonlinear figure of merit²⁸. Planar waveguides are longer than typical nonlinear crystal devices, but shorter than fiber based nonlinear devices, therefore the absolute device length is important, and high nonlinearity and dispersion tailoring are perhaps more important than loss.

The thermo-mechanical properties of the glass are important for fabricating fibers, and compound glasses exhibit far lower processing temperatures than silica, (typical compound glass softening temperatures are $\sim 500^\circ\text{C}$, as opposed to $\sim 2000^\circ\text{C}$ for silica), which enables the use of extrusion for fiber preform manufacture¹⁸. In addition, the low processing temperature facilitates the use of ceramic micro-heaters for compound glass fiber tapering, in contrast to CO₂ laser or flame burners used for silica taper fabrication²⁹.

Fiber tapering is an attractive option for non-silica glasses since it enables post-processing to fine tune the dispersion characteristics without requiring new fibers to be drawn. Mid-IR continuum generation has been demonstrated using a Bismuth fiber taper²⁹. Using a silica MOF, tapering has also been used for dispersion micro-management starting with a small core fiber and then tapering to shift the ZDW to shorter wavelengths³⁰. This technique enabled enhancement of spectral power generation in a variety of wavelength ranges, and should also be applicable to non-silica MOFs in the future.

The emergence of MOF fabrication technology is particularly enabling for multi-component glasses as it eliminates the need for two thermally, chemically and optically compatible glasses to form the fiber core and cladding as required for conventional step-index fibers. MOF technology thus provides a simple and convenient route to realizing fibers in high nonlinearity glasses that otherwise might not be able to be drawn into fiber form. Recent progress in extruded bismuth-oxide based glasses has been particularly noteworthy³¹, and we have also reported lead-silicate MOFs (Schott SF57 glass) using extrusion⁷, and the stacking technique³². An As-Se MOF has been reported that generated IR supercontinuum extending from 2.1-3.2 μm using 2.5 μm pumping³³.

Two main techniques have been used to fabricate compound glass MOFs¹⁸. One approach is to manually stack capillary tubes to produce the structured preform. This is the approach that is routinely used to produce silica microstructured fibers, and the resulting fibers typically consist of a hexagonal lattice of air holes surrounding the fiber core. It is anticipated that using the flexibility of this approach fiber geometries could be designed to tailor the dispersion characteristics (for example to achieve lower dispersion slope), but at present this technique is not well developed for compound glasses.

A second fabrication approach that works well for compound glasses (that in general have lower melting points than silica) is to use extrusion to produce the structured preform from bulk glass billets. This technique has now been used to produce a broad range of fiber geometries in a number of compound glass materials including lead silicate³⁴, bismuth oxide³¹ and tellurite²⁶ glass. The geometry that has been used for many of these demonstrations is the so-called “wagon-wheel” (WW) fiber, which is a micron-scale solid core suspended by three long fine glass struts that optically isolate the core within a robust solid jacket. A scanning electronic microscope (SEM) image of a WW fiber is shown in the insert to Fig. 3. In the WW fiber, the size of the core can be adjusted during the drawing process by modifying the outer fiber diameter. These fibers can readily be made with small cores and high NA, leading to tight mode confinement, and thus high fiber nonlinearity.

3. SMALL CORE MICROSTRUCTURED FIBER DESIGNS

This section describes work on modeling the optical properties possible in compound glass microstructured fibers with the aim of identifying designs that are particularly suitable for supercontinuum generation. Designs are considered for small core fibers, for which the waveguide dispersion is large, and can dominate the material dispersion. In contrast, LMA fibers have a rather small waveguide contribution to the dispersion, and therefore we have not considered a detailed review of LMA fiber designs.

Small core high NA MOF designs in general allow a broad range of dispersive properties to be achieved (depending on the detailed choice of the fiber geometry). A number of modeling techniques can be used for predicting the effective mode area and fiber dispersion of MOFs. For this survey the orthogonal function technique has been chosen^{35,36}. The advantages of this choice are that it can accurately and efficiently scan a broad range of wavelengths and structures, the material dispersion can be included in the calculations *ab initio*, and it is an experimentally validated method for predicting the dispersion of real fiber structures from SEMs.

The WW geometry has been used for this initial investigation because, in addition to offering high nonlinearity, it is a geometry that has been demonstrated to be practical for fabrication and handling in a range of glasses. The WW geometry also restricts the parameter space that needs to be investigated to a single parameter for each glass type (i.e. the core diameter). We model the structure of a real fiber as taken from an SEM image of a typical WW fiber (see insert to Fig. 3. a)). For these small core MOFs, two pump wavelengths were considered: 1.55 μm and 2.0 μm . We performed preliminary modeling to provide an understanding of the dispersive properties that can be achieved in compound glass WW fibers and to identify combinations of glass choice and fiber design that give zero net dispersion (i.e. $D_{\text{MAT}} + D_{\text{WG}} \approx 0$) for the pump wavelengths of interest. As a starting point, three core diameters are considered: 2.5, 3.3 and 4.1 μm . These are “enclosed” core diameters: the diameter of the circle that just fits within the triangular WW core. (Others have considered smaller core sizes for visible continuum generation³⁷)

Note that all the results given here are for the fundamental mode, and our past experience indicates that 2-3 μm cores can be operated in an effectively single mode fashion. The glasses identified in Section 2 have linear refractive indices between 1.5 and 2.4. We begin this design work by considering the specific cases $n=1.8$ and 2.4. For these preliminary calculations, the material is not defined, and so the material dispersion (D_{MAT}) cannot be included in the calculations. Although this is not ideal, it provides a reasonable approximation to the waveguide dispersion at a fixed wavelength (and can be confirmed for specific glass selections). The calculated values of the waveguide dispersion (D_{WG}) obtained in this preliminary survey ranged from +55 to +118 ps/nm/km. Similar ranges of values for D_{WG} were achieved at both potential pump wavelengths. As expected, either decreasing the core diameter or increasing the refractive index act to decrease the effective mode area, and the use of designs with smaller cores, leads to larger D_{WG} values.

Only a few materials have a large enough material dispersion to counteract the waveguide dispersion of any of these designs for the case of 2.0 μm pumping (see Section 2). Of the glasses considered, the one glass that has sufficient material dispersion to achieve this is GLSO (an oxide variant of Gallium Lanthanum Sulphide glass). Compound glasses have large normal material dispersion at shorter wavelengths, and so using 1.55 μm pumping expands the range of potential glasses that could be used for this application to include most of the materials considered in Section 2. Hence WW fibers can be designed with high nonlinearity and zero dispersion for both 1.55 μm and 2.0 μm pumping arrangements (with a wider range of glasses offering zero net dispersion at 1.55 μm).

Following this preliminary modeling, fiber designs were iterated to provide zero net dispersion with the chosen Bi, and GLSO glasses (Section 2), and for 1.55 μm , and 2.0 μm pump schemes. The aim of this work is to predict the dispersion and effective area of these fibers in sufficient detail to allow the supercontinuum modeling described in the next section.

For 1.55 μm pumping we focus on the example of Asahi bismuth oxide glass (Bi) for 1.55 μm pumping. This glass has been used extensively for the fabrication of high quality WW fibers³¹. The linear refractive index of Bi is ≈ 2.02 and the material dispersion of Bi is -107 ps/nm/km at 1.55 μm . Interpolation of the data from the preliminary modeling survey suggested that an enclosed WW core size of $\approx 2.6 \mu\text{m}$ was required to achieve zero net dispersion at this wavelength. For this more detailed calculation, the linear refractive index for Bi was set using the fitted Sellmeier equation for this bismuth glass. Fig. 3 shows the calculated net dispersion (D) and effective mode area (A_{eff}) for this fiber calculated at a discrete set of wavelengths: 1.0, 1.33, 1.55, 2.0, 2.5, 3.0, 3.5, 4.0, 4.5 and 5.0 μm . Note that this calculation (in which the extrapolated core size and correct Sellmeier refractive index are used) shows that at 1.55 μm the net dispersion is indeed close to zero, in agreement with the prediction of the preliminary study. The shape of the dispersion curve at the other wavelengths shown will have an impact on the generation of supercontinuum, and this is explored further in Section 4.

For 2.0 μm pumping, as noted above, only GLSO has the material dispersion required to counteract the WW fiber waveguide dispersion at 2.0 μm . Again, linear interpolation of the preliminary results was used to select the most appropriate enclosed core dimension (in this case 3.5 μm) for these detailed calculations. Note that such a fiber would be expected to be multimode. Fig. 3 shows the calculated net dispersion (D) and mode area (A_{eff}) for this fiber. Again, this more accurate calculation (in which the correct Sellmeier refractive index is used) confirms that at 2.0 μm , the net dispersion is near zero.

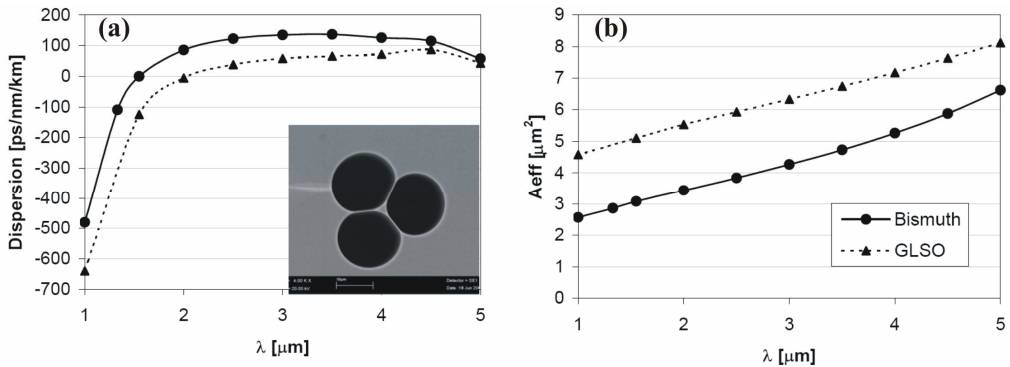


Fig. 3. a) Dispersion for 2.6 μm core Bi and 3.5 μm core GLSO WW fiber. b) Effective mode area (A_{eff}) for small core Bi and GLSO WW fiber. The inset shows an SEM of a typical WW fiber.

The fiber dispersion shows a very strong variation with wavelength due to the strong waveguide contribution, whereas A_{eff} is a more slowly varying function of wavelength. However, the GLSO fiber dispersion is lower and flatter than that of Bi fiber throughout the mid-IR. The A_{eff} of the GLSO fiber is larger than that of Bi, which tends to reduce the nonlinearity, but since the material nonlinearity of GLSO is ~ 6 times larger than Bi, overall the GLSO fiber has larger nonlinearity.

4. SUPERCONTINUUM SIMULATIONS

To predict the supercontinuum spectra that would be possible from each of the fibers considered, we performed numerical simulations. The heavy-metal-oxide glasses are more technologically developed than the highest nonlinearity sulfide glasses, so we have used the small core Bi MOF (described in section 3) as a base-case for our investigation. Supercontinuum generation depends on the interplay between seed pulse (energy, duration, wavelength), and fiber (length, dispersion, nonlinearity, loss). We studied the changes in the continuum resulting from changes in the dispersion, nonlinearity, and loss; for example, we compared the spectrum from a simulation that used the measured loss of the fibers, to the spectrum from a simulation without fiber loss.

The limits on the range of pulse energy and fiber nonlinearity were the maximum values that could be simulated without causing numerical instabilities (using an increase in pulse energy as a benchmark). In an experiment, the maximum physical value of intrinsic nonlinearity would be limited by the available glasses. The maximum pulse energy could be limited by the available pump laser or the material damage threshold. Indeed, input facet damage has been reported when launching pulses with similar duration and energy to those considered in this study when using small core silica MOF for visible/UV supercontinuum experiments^{12,38,39} (although the precise damage mechanism was not identified). We might therefore expect that in future experiments fiber facet damage may occur for multi-component glass MOF unless care is taken to minimize perturbations at the fiber launch, but at present we have no detailed data on damage thresholds for the particular glasses considered.

We first describe the numerical model used for the simulations in section 4.1. Simulation results for various seed pulse energies, and pulse durations are presented in section 4.2. Simulation results for different fiber dispersion profiles are compared in section 4.3. The spectra from different fiber nonlinearities and with the other properties of the reference Bi WW MOF are shown in section 4.4. That section also considers the spectrum predicted for the GLSO WW MOF. The significance of fiber loss is shown in section 4.5. Section 4.6 shows simulations for large mode fibers.

Seeding with ~ 200 fs pulses close to the fiber's ZDW, the mechanism for supercontinuum generation is by soliton fission³. Over a typical propagation distance of only a few cm, the initial pulse undergoes nonlinear compression, soliton fission, and then rapid spectral broadening. The high dispersion values experienced by the newly generated wavelengths result in temporal broadening, and reduced peak power. The supercontinuum width therefore saturates after this threshold length, as has been previously reported⁴⁰. We have consistently compared fully evolved spectra beyond this threshold length, and the differences between observed spectra were thus attributed to dispersion, nonlinearity, and loss. In contrast to the results presented here, with longer duration seed pulses e.g. >50 ps, the dominant mechanisms for spectral broadening are self-phase-modulation (SPM) and four-wave-mixing (FWM)^{28,41}. Therefore a separate study would be required to predict the spectra and particularly the appropriate fiber lengths with much longer seed pulses.

The predicted spectra in all graphs that follow are shown using a dBm/nm scale, assuming a pulse repetition rate of 1 Hz. This scale would show an average power of 0 dBm/nm for 1 mJ pulses with 1 nm spectral widths. Scaling the power spectra to different pulse repetition rates can be done as follows: e.g. starting with -70 dBm/nm at 1 Hz, and converting to 1 MHz (10^6 Hz) gives $(-70+60) = -10$ dBm/nm.

4.1 Numerical model

As with silica, we have assumed that the amorphous multicomponent glasses are centro-symmetric, and therefore have no second order nonlinear susceptibility ($\chi^{(2)}$), and have a homogeneous third order nonlinear susceptibility ($\chi^{(3)}$). The third order nonlinear susceptibility is assumed to be small compared to the linear susceptibility, and is also assumed to be wavelength independent over the wavelength range considered in this paper. The total refractive index therefore includes a small intensity dependent nonlinear contribution: ($n = n_0 + n_2 I$). Effects such as two photon absorption have not been included. Furthermore, since single mode operation is often observed in MOF, we have considered only processes occurring within the fundamental fiber mode, and not mode-mixing to possible higher order modes. These simplifications enable modeling of the pulse-propagation using the modified nonlinear Schrödinger equation (NLSE) with loss²⁸, as shown below:

$$\frac{\partial A}{\partial z} - i \sum_{k \geq 2} \frac{i^k \beta_k}{k!} \frac{\partial^k A}{\partial t^k} + \frac{\alpha(\omega)}{2} A = i\gamma \left(1 + \frac{i}{\omega_0} \frac{\partial}{\partial t} \right) \left(A(z,t) \int_{-\infty}^{+t} R(t') |A(z,t-t')|^2 dt' \right),$$

where $\gamma = (n_2 \omega_0 / c A_{eff})$, $A(z,t)$ is the electric field envelope, β_k are the dispersion coefficients at the centre frequency, ω_0 , and $\alpha(\omega)$ is the frequency dependent fiber loss. The full wavelength dependent loss of the fibers was included as shown in section 2. We also used the full wavelength dependent dispersion data from Fig. 3 (small core fibers) and from Fig. 2 (large mode fibers). We used the A_{eff} data from section 3 as calculated at the seed pulse wavelength. To solve the propagation equation, we used a standard split-step Fourier algorithm treating dispersion in the frequency domain and the nonlinearity in the time domain, apart from the temporal derivative for the self-steepening effect, which was evaluated using Fourier transforms.

The model includes both the instantaneous electronic response (responsible for the Kerr effect), and the delayed ionic response (responsible for Raman and Brillouin scattering) in the nonlinear component of the refractive index, n_2 . As is usual when modeling silica fibers, the nonlinear response to the applied field, $A(z,t)$, has been written as $R(t) = (1 - f_R) \delta(t) + f_R h(t)$, where the δ -function represents the instantaneous electronic response and $h(t)$ represents the delayed Raman response of the ions. The modified NLSE has been used by other authors for the numerical study of supercontinuum generation^{10,11}.

We note that there are further refinements that can be made to the above NLSE to include effects such as polarisation coupling, and the wavelength dependence of A_{eff} , but the simulations should provide a reasonable estimate of the expected spectra. Our simulation results show the expected fine structuring¹⁰ and we have applied a rolling average to smooth the spectra. These smoothed spectra should be approximately comparable to the time average over several pulses that would be measured in experiments in which the seed pulses have small energy fluctuations. The simulated seed pulse was taken to be a transform limited Gaussian profile at the relevant centre wavelength.

4.2 Simulations for various seed pulses with different energy and duration

For the reference example of small core Bi WW MOF described in section 3, we performed simulations with fiber length of 40 mm, and pulses having $\lambda_{seed} = 1.55 \mu\text{m}$ (\approx fiber ZDW), $T_0 = 0.2$ ps (FWHM), and pulse energies of $E_0 = 0.1, 0.25, 0.5, 1, 2, 4$ nJ. The loss was set to zero for these simulations, so the broadening is controlled only by dispersion and nonlinearity. The spectra in Fig. 4 (a) shows that there was only limited spectral broadening for 0.1 nJ pulses, but for all pulse energies > 0.5 nJ the supercontinuum generation extended to $\lambda = 2.5 \mu\text{m}$. Increasing the energy to 4.0 nJ led to further broadening of the spectrum to $\lambda = 3.0 \mu\text{m}$.

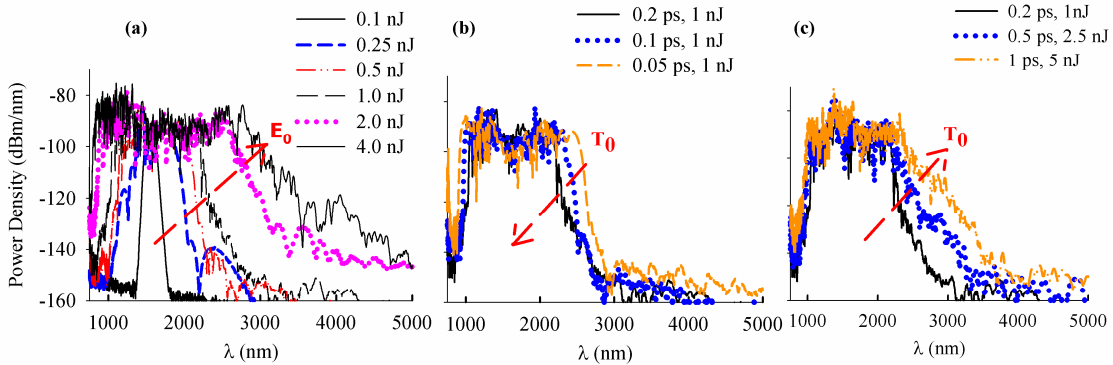


Fig. 4. Variation of supercontinuum spectra with seed pulse energy and duration for small core Bi MOF. ($\lambda_{seed} = 1.55 \mu\text{m}$, and fiber length=40 mm, loss = 0 dB/m). (a) Increasing seed pulse energy ($T_0 = 0.2$ ps). (b) Increasing pulse duration: $T_0 \leq 0.2$ ps ($E_0 = 1$ nJ). (c) Increasing pulse duration: $T_0 \geq 0.2$ ps, and with E_0 increased to maintain a constant peak power (E_0/T_0).

Simulations were then performed for initial pulse durations of $T_0 = 0.05, 0.1, 0.2, 0.5, 1$ ps, with E_0 fixed at 1.0 nJ. The fiber loss was again set to zero for these simulations. The results for pulse durations ≤ 0.2 ps are shown in Fig. 4 (b). The shorter pulses produced a spectrum with approximately 200 nm additional broadening compared to $T_0 = 0.2$ ps

pulses. For seed pulses with $T_0 > 0.2$ ps, narrower spectra resulted (not shown) unless the seed pulse energy was scaled up in proportion to T_0 to maintain constant initial peak power, in which case the spectrum broadened by an additional ~ 400 nm at a level 20 dB below the peak as shown in Fig 4 (c).

We concluded that for this reference fiber, using pulses with seed wavelength of $\lambda = 1.55 \mu\text{m}$, $E_0 = 1$ nJ, and $T_0 = 0.2$ ps would be suitable for testing the importance of dispersion, nonlinearity, and loss, and these seed pulse parameters were used as the reference case for the simulations that follow.

4.3 Simulations demonstrating the significance of fiber dispersion

The fiber dispersion can have a strong influence on the shape of the supercontinuum spectrum. Considering the pulse evolution in the time-domain, normal dispersion tends to broaden the pulse duration, which decreases the peak power and gradually reduces the rate of nonlinear phase generation. In contrast, anomalous dispersion combined with nonlinearity can lead to soliton formation, and if higher order solitons are generated, soliton fission then leads to rapid spectral broadening.

To assess the sensitivity of the supercontinuum broadening to modest changes in the dispersion profile, we performed simulations with all fiber parameters held constant except for the dispersion profile. We calculated the dispersion of a circular core Bi MOF with variable core radii and variable index contrast between core and cladding as it is well known that varying these parameters for a silica MOF can lead to a wide variety of dispersion profiles³⁵. The fiber designs maintained a fixed lower ZDW at $1.55 \mu\text{m}$, and have a second ZDW at longer wavelengths as shown in Fig. 5. (a). The choice of dispersion was in order to maintain a fixed relation between the pump wavelength and lower ZDW. While other choices of flattened dispersion profile are possible, the fiber designs chosen provided insight into the importance of the overall shape of the dispersion profile, rather than variations in the relation of the pump and ZDW. For these simulations the fiber length was 40 mm, and the fiber loss was again set to zero. For a similar study of the influence of dispersion variation in silica MOF for visible continuum generation, see Frosz *et al*⁴².

The resulting spectra are shown in Fig. 5 (b). At shorter wavelengths, there is minimal variation which is probably due to the steep dispersion profiles, which are inherent to the waveguide dispersion of small-core, high-air-fill MOF designs required to move the bulk material ZDW of $>2 \mu\text{m}$ to the Er-pump wavelength of $\sim 1.55 \mu\text{m}$. For the dispersion profiles that have maxima significantly lower than the WW dispersion maximum and two closely spaced ZDWs, the spectrum broadens to $3.0\text{-}3.5 \mu\text{m}$ by phase-matching to wavelengths above the second ZDW where the dispersion is normal. A more detailed study of the effects of varying the dispersion profile might also consider dispersion flattened designs which, over longer fiber lengths, may broaden the mid-IR spectrum by the soliton-self-frequency shift. We concluded that the dispersion profile of the small core Bi WW MOF was limiting the supercontinuum broadening to $\sim 2.2 \mu\text{m}$, and that a fiber with more a complex cladding structure, which was designed to accommodate a smaller air-fill fraction, could provide a dispersion profile that would lead to a broader mid-IR continuum.

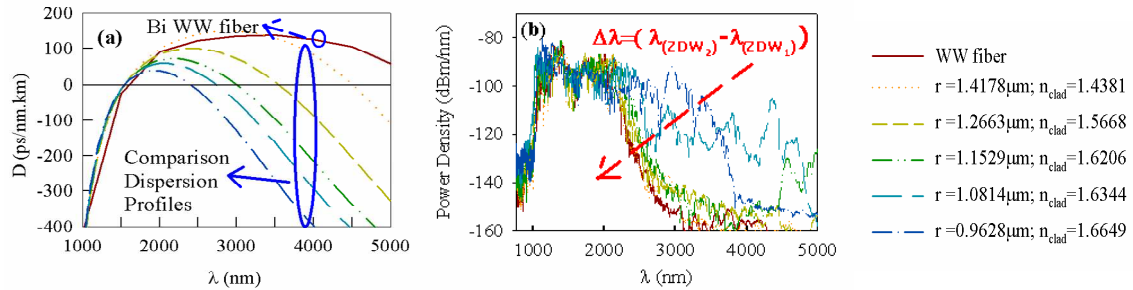


Fig. 5. (a) Dispersion profile of Bi WW fiber and of Bi glass circular rods (fiber cores) with variable radius and surrounding average refractive index shown in the graph caption. (b) Spectra for Bi MOF using the dispersion profiles shown in (a). ($\lambda_{\text{seed}} = 1.55 \mu\text{m}$, $E_0 = 1$ nJ, $T_0 = 0.2$ ps, fiber length = 40 mm, loss = 0 dB/m.)

4.4 Simulations for increased intrinsic nonlinearity of the glass

Compound glasses have a wide range of intrinsic nonlinearity values as shown in Table 1 of section 2. This section investigates the effects of changing the nonlinear response of the glass. Starting again with Bi WW fiber as a reference,

simulations were performed with increased n_2 values to demonstrate the extent the nonlinearity can influence the continuum. This section also shows additional simulation results for GLSO small core MOF, an example of a glass with very high intrinsic nonlinearity (Table 1) which was designed for pumping at $2.0\ \mu\text{m}$ as described in section 3.

We are not aware of previous measurements of the delayed Raman responses of these multi-component glasses. For silica, the Raman temporal response $h(t)$ has been previously determined from the shape of the Raman gain in the frequency domain⁴³, and $f_R=0.18$ was determined from measurements of the absolute value of the Raman gain. We calculated the shape of the delayed temporal responses of the multi-component glasses studied here from uncalibrated spontaneous Raman spectra measured by the authors, and then following the procedure used by Stolen *et al*⁴⁴ for silica. We have assumed that $f_R=0.2$, based on the known fraction of 0.18 for silica.

Fig. 6 (a) shows the spectra from simulations performed for Bi WW fiber for the same seed pulse parameters and with: (i) SPM term only, (ii) SPM and self-steepening terms, and (iii) including the Raman response. The fiber loss was set to zero for all simulations shown in this section. The overall shape of the continuum is similar in all cases, and there is a small decrease in the extent of the continuum with the self-steepening term and with the Raman response when compared to pure SPM nonlinearity. We concluded that the continuum generation is not highly dependent on the Raman response in this fiber, and therefore whilst the exact value of f_R is uncertain for these glasses, small differences from the assumed value of 0.2 should perhaps lead to only small changes to our predicted spectra.

To show the influence of the magnitude of the material nonlinearity, simulations were performed using $1 \times n_2$ of Bi, $2 \times n_2$, $4 \times n_2$, and $6 \times n_2$, and the spectra are shown in Fig. 6. (b). For $6 \times n_2$, the continuum extends to $\sim 3.5\ \mu\text{m}$. As a reference to a physical glass with this nonlinearity, $6 \times n_2$ of Bi $\approx n_2$ of GLSO. We concluded that increasing the material nonlinearity has a similar influence to increasing the pulse energy, and leads to modest additional broadening. However, the influence of the nonlinearity appeared to be less significant than that of the dispersion profile.

The continuum produced by the GLSO WW MOF pumped at $2.0\ \mu\text{m}$ is shown in Fig. 8 (a). The spectrum significantly broader than for the Bi WW MOF and extends to $\sim 4\ \mu\text{m}$. The GLSO fiber has both an increased intrinsic nonlinearity, and a lower, flatter dispersion profile through the mid-IR.

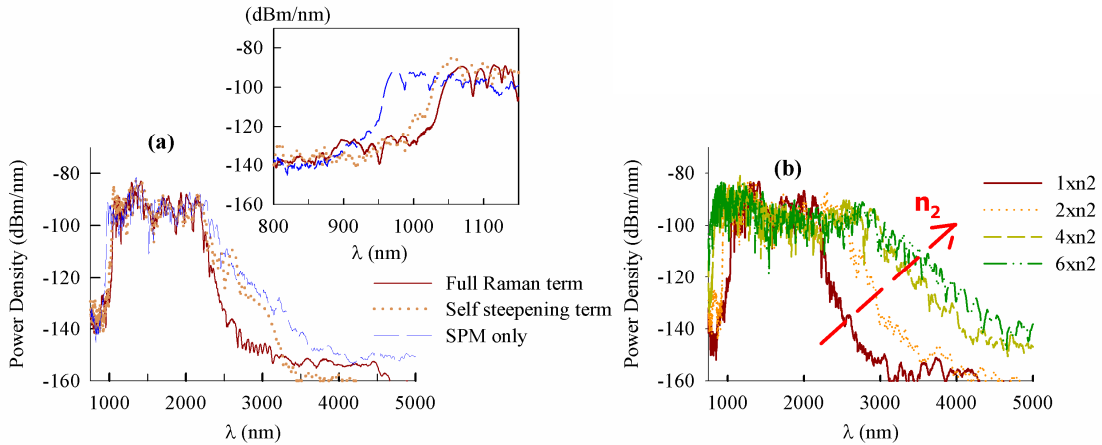


Fig. 6. Spectra for small core Bi MOF. (a) Variation due to Raman response component of total nonlinearity, compared to pure SPM, and SPM combined with self-steepening effect. (b) Variation due to increasing material nonlinearity. Nonlinear index = $1 \times$, $2 \times$, and $6 \times n_2$ of Bi. (The Raman response is included in these simulations with $f_R=0.2$.) (For both (a) and (b), fiber length = 40 mm, loss = 0 dB/m, $\lambda_{\text{seed}} = 1.55\ \mu\text{m}$, $E_0 = 1\ \text{nJ}$, $T_0 = 0.2\ \text{ps}$).

4.5 Simulations demonstrating the significance of fiber loss

The simulations above demonstrated that the fiber lengths required for supercontinuum generation are short, being $< 40\ \text{mm}$, and that even without including loss, the spectrum from Bi WW MOF did not extend beyond $\sim 3.3\ \mu\text{m}$ due to the dominant influence of the dispersion profile. Therefore, only once a suitable combination of seed pulse, dispersion profile, and effective nonlinearity are selected would the spectrum be limited by loss. Fig. 7. shows the reference case Bi WW MOF spectrum with and without the measured absorption loss, and there is negligible difference due to loss. The

OH loss peak is shown for reference, calculated by taking the difference in loss of normal and dehydrated Bi samples shown in Fig. 1 (b). In order to see any significant difference on the spectrum, Fig. 7 (b). shows the effects of loss when using seed pulse energy increased to 4 nJ. There is >25 dB reduction in power at $\sim 3.2 \mu\text{m}$ due to the loss peak.

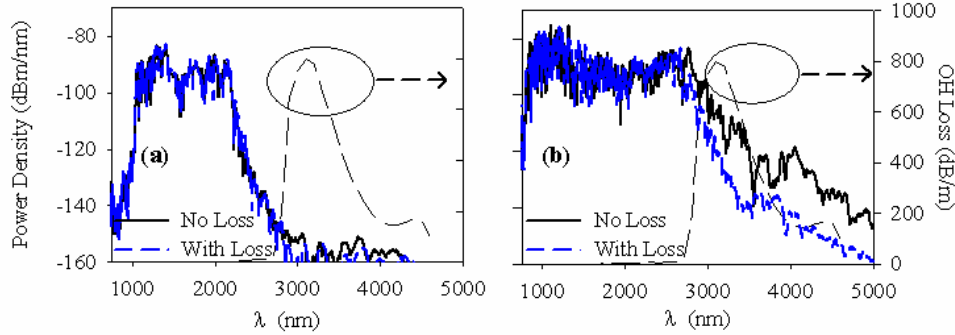


Fig. 7. (a) Variation of continuum due to loss for Bi WW MOF, $E_0 = 1 \text{ nJ}$. (b) Variation of continuum due to loss for Bi WW MOF, $E_0 = 4 \text{ nJ}$. (For (a) and (b) $\lambda_{\text{seed}} = 1.55 \mu\text{m}$, $T_0 = 0.2 \text{ ps}$, length = 40 mm).

Small core MOFs of the type considered in this paper typically show waveguide losses of $\sim 2 \text{ dB/m}$ (in addition to the material loss), due to scattering from core surface roughness and contaminants accumulated during fabrication. In addition, all modes of a MOF have an associated confinement loss (due to the finite extent of the cladding region)⁴⁵, but these losses can be reduced to low values by ensuring a sufficiently large microstructured cladding region. Therefore, the total fiber losses would be dominated by the rather high material losses and with the short lengths of fiber considered in this paper, the waveguide related losses can be considered to be negligible.

As shown in section 2, for all of the non-silica glasses considered, the intrinsic (phonon) loss edge is above the maximum wavelength of the predicted supercontinuum spectra shown above. Oxide based glasses including Schott SF57 (lead oxide) and tellurite glasses can have strong OH absorption losses in the wavelength range $3.0\text{-}3.5 \mu\text{m}$, but these extrinsic losses can be reduced to $< 100 \text{ dB/m}$ by dehydration processes. Since oxide glasses have similar inherent nonlinearity characteristics, we suggest that dehydration processes should be applied to reduce the OH absorption peak for these glasses, but that the trends for the supercontinuum broadening shown for Bi above, when changing E_0 , T_0 , dispersion, and nonlinearity would again apply when losses were included. (The simulations in the previous sub-sections were performed without including any losses.) If a different pump wavelength and dispersion profile enabled the supercontinuum to extend to the phonon absorption edge, then the effect of loss on the spectrum should be reconsidered. If dehydrated samples are not available, then the fiber length should be minimized, and tapers, which are typically $\geq 100 \text{ mm}$ long, could be less favourable. For sulfide glasses, the OH absorption peak can be as low as 10 dB/m , so it would have a minor impact on the spectra.

4.6 High power mid-IR continuum using large mode fibers

In order to increase the pulse energy it becomes necessary to work with fibers with a larger core area in order to avoid material damage. In selecting an appropriate mode area for simulations, we observed that for silica MOF, the largest single mode fiber available has $A_{\text{eff}} \sim 1000 \mu\text{m}^2$ (Crystal Fibre A/S DC-170-40-Yb). Non-silica glasses have larger refractive indices compared to silica, and are more challenging to fabricate, so achieving the precision necessary for such a large mode area (LMA) would probably be very challenging for current technology. Therefore as a reference case, we simulated the supercontinuum for an $A_{\text{eff}} \sim 100 \mu\text{m}^2$ Bi fiber. (This A_{eff} does not correspond to a particular design, but is representative of what might be suitable for a low NA fiber that has approximately single mode operation.) The $100 \mu\text{m}^2$ mode area is ~ 30 times greater than for the small core Bi fiber considered above, and the LMA fiber has correspondingly reduced effective nonlinearity. We used the same seed pulse duration of 0.2 ps as for the small core simulations and we maintained approximately the same initial peak intensity by scaling the pulse energy by the ratio of the mode areas: $(100 \mu\text{m}^2 / 3.05 \mu\text{m}^2) \times 1 \text{ nJ} \approx 30 \text{ nJ}$.

Since the LMA fiber dispersion is almost equal to the material dispersion, changing dispersion profile requires the use of a different glass, which would also have different intrinsic nonlinearity. For this survey, we therefore considered Bi, SF57 and GLSO to demonstrate the range of spectra from LMA fibers. The seed pulse wavelength should again be close

to the fiber ZDW to obtain efficient continuum generation. We chose a seed wavelength of $2.25\ \mu\text{m}$, for which the dispersion of SF57, Bi and GLSO is respectively: low and anomalous, ≈ 0 , and high and normal, as shown in Fig. 2 (b).

The spectra in Fig. 8 (b) were generated with identical seed pulses and therefore show possible spectra for a fixed pump system, and the spectra extend to $\sim 3.5\ \mu\text{m}$ for both Bi and SF57, and to $\sim 3.8\ \mu\text{m}$ for GLSO. Although the dispersion profile and seed wavelength are more favourable for Bi and SF57, the much higher nonlinearity of GLSO glass resulted in a similar broadening of the continuum at long wavelengths for all the fibers. In comparison with the small core MOF spectra a significant difference in the LMA spectra is the extension to longer wavelengths. The broader LMA fiber spectra are due mainly to the dispersion profile, which is dominated by the gently sloping material dispersion, whereas for the small core MOFs considered earlier, the steep waveguide dispersion dominates. Since it should be possible to use dehydrated glasses in experiments and because the fiber lengths are short, the spectra are not likely to be significantly affected by loss.

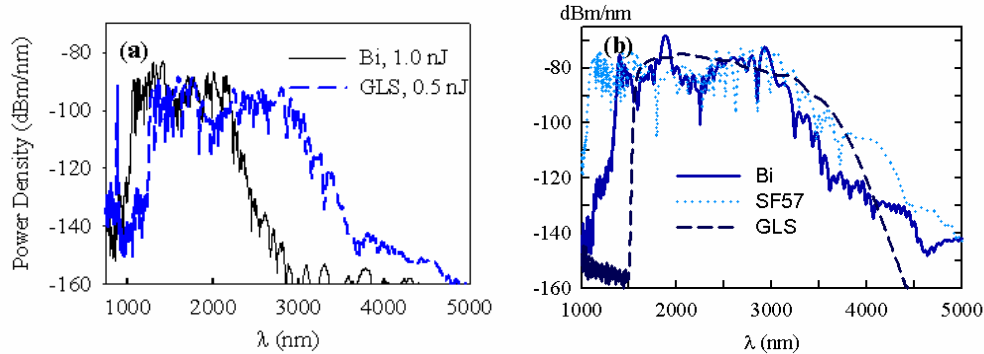


Fig. 8. (a) Supercontinuum spectra predicted for small core Bi and GLSO MOF. (Fiber length = 40 mm, loss = 0 dB/m, $T_0=0.2$ ps. Bi MOF: $\lambda_{\text{seed}} = 1.55\ \mu\text{m}$, $E_0=1.0$ nJ. GLSO MOF: $\lambda_{\text{seed}} = 2.0\ \mu\text{m}$, $E_0=0.5$ nJ.) (b) Supercontinuum spectra predicted for Bi, SF57, and GLSO LMA fibers. (Fiber length = 40 mm, loss = 0 dB/m, $T_0=0.2$ ps, $E_0=30$ nJ, $\lambda_{\text{seed}} = 2.25\ \mu\text{m}$.)

The GLSO LMA continuum was smooth because the dispersion is normal at wavelengths below $3.2\ \mu\text{m}$, so the continuum is due to SPM, and the continuum would have good temporal coherence for applications including pulse compression and metrology. The SPM generated spectral broadening in the GLSO LMA fiber would be expected to increase steadily with the initial pulse peak power, which is different to our findings for anomalously dispersive fibers for which the soliton-fission mechanism causes the continuum broadening to saturate above a given seed pulse energy. Pumping GLSO at longer wavelengths, hence closer to the ZDW, should produce broader continuum, and therefore for high power continuum beyond $3.5\ \mu\text{m}$ this is the preferred glass.

Non-silica LMA fibers are therefore shown to be promising for high power mid-IR sources, with the highest nonlinearity sulfide glasses likely to produce the broadest spectra using pump wavelengths $\sim 2.5\ \mu\text{m}$. The pump requirements are for higher energy pulses compared to small core MOFs due to the larger mode. The dominance of the material dispersion over the much smaller waveguide contribution also requires pumping at longer wavelengths compared to small core MOFs, for which the ZDW can be tailored to the pump source.

5. SUMMARY AND CONCLUSIONS

In this paper we have performed numerical simulations to study mid-IR supercontinuum generation in MOFs made from multi-component glasses when pumped with 0.2 ps pulses at wavelengths below $2.25\ \mu\text{m}$. We considered two broad categories of multicomponent glass, the first of which includes heavy metal oxide, gallate and tellurite glasses, with nonlinearities ~ 10 x that of silica. The second category includes sulfide glasses, which have even higher nonlinearities.

Using a Bi WW MOF as an example, we performed simulations in which the dispersion, nonlinearity and loss were separately varied in order to demonstrate desirable combinations of fiber characteristics for broad supercontinuum generation. The fiber lengths required for mid-IR continuum were ~ 40 mm for all the glasses, so the losses of the fibers were not a limiting factor. (We note that for fiber based transmission of supercontinuum after generation, much longer fibers would be used, and therefore the material loss would perhaps dominate other considerations, but this issue has not

been considered in this paper.) In addition, our results showed that over the range of parameter values considered, the nonlinearity due to the Raman response was not a key factor in controlling the continuum. The continuum extended to $\sim 3.0 \mu\text{m}$, but further broadening was prevented by the steep dispersion profile. The initial simulations provided insight about which parameters of the fibers strongly influenced the mid-IR supercontinuum. The most important parameter was the overall dispersion profile across the mid-IR. The simulation results using fiber designs with two ZDWs (produced using more complex structures than the WW design) suggest that most multi-component glasses could produce $2\text{-}3 \mu\text{m}$ supercontinuum with $1.55 \mu\text{m}$ pumping when using appropriately designed fibers. Using a glass with shorter wavelength material ZDW than Bi, it should be possible to create a MOF with flatter dispersion profile to extend the mid-IR broadening possible from a $1.55 \mu\text{m}$ source e.g. SF57 has a shorter wavelength $\text{ZDW}_{\text{Material}}$ than Bi (and also a higher material nonlinearity). Considering the much higher nonlinearity sulfide category of glasses, the material ZDW is at $>3 \mu\text{m}$ so it is less likely that sulfide glasses would be suitable for pumping at this wavelength. LMA fibers fabricated from the glasses considered would have very high normal dispersion at $1.55 \mu\text{m}$ (Fig. 2 (b)) and would not produce continuum efficiently with this seed wavelength.

Pumping small core fibers at wavelengths in the range $1.55\text{-}1.9 \mu\text{m}$, similar considerations would apply compared to $1.55 \mu\text{m}$ pumping, and the most promising fibers are small core MOFs made of oxide glasses. However, since the pump wavelength is closer to the ZDW of the material, dispersion flattened fibers should be possible, and we might expect significantly more broadening using optimised dispersion design algorithms previously developed for silica-based MOF fabrication⁴⁶ to develop suitable fiber structures for compound glasses. Since the material damage thresholds of the glasses are not yet well understood, reducing the threshold peak intensity required for continuum generation could be an important practical consideration.

Pump wavelengths of $2.0\text{-}2.5 \mu\text{m}$ are close to the material ZDW of the oxide glasses. Therefore because small core MOF designs tend to result in a shift of the ZDW to shorter wavelengths, which are further from the pump wavelength, small core fibers made from the oxide glasses are probably not well suited to these pump wavelengths. The ZDW of the high nonlinearity glasses is still above this wavelength range, but small core MOFs could move the overall fiber ZDW close to the pump wavelength, and the results of section 4.4 suggest that such fibers should produce broad continuum.

We then extended the survey to large mode fibers which have dispersion properties close to those of the bulk glasses. For pumping in the $1.55\text{-}1.9 \mu\text{m}$ wavelength range LMA fibers appear to have unfavourable dispersion properties. For pump wavelengths of $2.0\text{-}2.5 \mu\text{m}$, LMA fibers made from oxide glasses should produce continuum extending beyond $3.5 \mu\text{m}$ due to the favourable match to the material dispersion profile. Although the ZDW of the high nonlinearity sulfide glasses is less well matched to these pump wavelengths, simulations showed that such fibers produce similar continuum broadening and the continuum from high nonlinearity sulfide LMA fibers would have high temporal coherence as it is generated in the normal dispersion region. Pumping above $2.5 \mu\text{m}$, most oxide glasses are hard to optimize in LMA fiber designs because they would have shorter wavelength ZDWs. The high nonlinearity sulfide glasses would be promising in both small core dispersion flattened designs for low pulse energy sources, and in LMA fibers for high power applications. However, given the present lack of data about material properties at such long wavelengths, the shape of the supercontinuum produced should perhaps be considered in a future study once more data becomes available.

Based on the results of this study, which used fiber parameters available from demonstrated fiber technology, and with readily obtainable seed pulse energies, we suggest that efficient mid-IR supercontinuum sources should be possible in the near future based on non-silica MOF technology. Highly efficient low power sources could be based on sub-picosecond pulsed sources with energies $\sim 1 \text{ nJ}$ in the $1.55\text{-}2.0 \mu\text{m}$ wavelength range, coupled into fibers fabricated from a range of high-nonlinearity oxide or sulfide glasses and using small core MOF designs with tailored dispersion. Efficient high-power sources using LMA MOFs could be created using sub-picosecond, $\geq 30 \text{ nJ}$ pump sources at wavelengths above $2.0 \mu\text{m}$ for which $\lambda_{\text{seed}} \approx \text{ZDW}_{\text{Material}}$. Compared to planar rib-waveguides or fiber-tapers, microstructured fiber technology has the advantages of greater flexibility for tailoring the dispersion profile over broad a wavelength range, and a much wider possible range of device lengths.

ACKNOWLEDGEMENTS

This work was undertaken with funding from BAE SYSTEMS Virtual University (UK). We thank R. Paschotta of RP Photonics Consulting (www.rp-photonics.com) for providing his ProPulse software for pulse propagation modeling. We acknowledge helpful discussions with Dr. D. Hewak, Dr. A. Favre, and Dr. P. Horak.

REFERENCES

- 1 J. K. Ranka, R. S. Windeler, and A. J. Stentz, "Visible continuum generation in air-silica microstructure optical fibers with anomalous dispersion at 800 nm," *Opt. Lett.* **25** (1), 25-27 (2000).
- 2 A. V. Husakou and J. Herrmann, "Supercontinuum generation of higher-order solitons by fission in photonic crystal fibers," *Phys. Rev. Lett.* **87**, 203901 (2001).
- 3 J. Herrmann, U. Griebner, N. Zhavoronkov et al., "Experimental evidence for supercontinuum generation by fission of higher-order solitons in photonic fibers," *Phys. Rev. Lett.* **88**, 173901 (2002).
- 4 P. Petropoulos, T. M. Monro, W. Belardi et al., "2R-regenerative all-optical switch based on a highly nonlinear holey fiber," *Opt. Lett.* **26** (16), 1233-1235 (2001).
- 5 R. Holzwarth, T. Udem, T. W. Hansch et al., "Optical frequency synthesizer for precision spectroscopy," *Phys. Rev. Lett.* **85** (11), 2264-2267 (2000).
- 6 I. Hartl, X. D. Li, C. Chudoba et al., "Ultrahigh-resolution optical coherence tomography using continuum generation in an air-silica microstructure optical fiber," *Opt. Lett.* **26** (9), 608-610 (2001).
- 7 Julie Y.Y. Leong, Periklis Petropoulos, Symeon Asimakis et al., *A lead silicate holey fiber with $\gamma=1860\text{ W}^1\text{km}^{-1}$ at 1550 nm*, Optical Fiber Communications Conference (OFC), Los Angeles, California, USA, paper PDP22., 2005.
- 8 J. H. V. Price, W. Belardi, T. M. Monro et al., "Soliton transmission and supercontinuum generation in holey fiber, using a diode pumped Ytterbium fiber source," *Opt. Express* **10** (8), 382-387 (2002).
- 9 H. Hundertmark, D. Kracht, D. Wandt et al., "Supercontinuum generation with 200 pJ laser pulses in an extruded SF6 fiber at 1560 nm," *Opt. Express* **11** (24), 3196-3201 (2003).
- 10 J. M. Dudley and S. Coen, "Coherence properties of supercontinuum spectra generated in photonic crystal and tapered optical fibers," *Opt. Lett.* **27** (13), 1180-1182 (2002).
- 11 G. Genty, M. Lehtonen, H. Ludvigsen et al., "Spectral broadening of femtosecond pulses into continuum radiation in microstructured fibers," *Opt. Express* **10** (20), 1083-1098 (2002).
- 12 J. H. Price, T. M. Monro, K. Furusawa et al., "UV generation in a pure silica holey fiber," *Appl. Phys. B-Lasers Opt.* **77** (2), 291-298 (2003).
- 13 Julie Y.Y. Leong, Periklis Petropoulos, Jonathan H.V. Price et al., "High-nonlinearity, dispersion-shifted lead-silicate holey fibers for efficient 1 μm pumped supercontinuum generation," *J. Lightwave Technol.* (**accepted**) (Accepted) (2005).
- 14 D. J. Brady, T. Schweizer, J. Wang et al., "Minimum loss predictions and measurements in gallium lanthanum sulphide based glasses and fibre," *J. Non-Cryst. Solids* **242** (2-3), 92-98 (1998).
- 15 P. W. France, S. F. Carter, M. W. Moore et al., "Progress in fluoride fibres for optical communications," *Br. Telecom. Technol. J.* **5**, 28-44 (1987).
- 16 www.amorphousmaterials.com.
- 17 www.coractive.com.
- 18 M. Feng, A. K. Mairaj, D. W. Hewak et al., "Nonsilica glasses for holey fibers," *J. Lightwave Technol.* **23** (6), 2046-2054 (2005).
- 19 *data provided by Asahi Glass Co.*
- 20 www.schott.com.
- 21 E. M. Vogel, M. J. Weber, and D. M. Krol, "Nonlinear Optical Phenomena in Glass," *Phys. Chem. Glasses* **32** (6), 231-254 (1991).
- 22 S. Fujino and K. Morinaga, "Material dispersion and its compositional parameter of oxide glasses," *J. Non-Cryst. Solids* **222**, 316-320 (1997).
- 23 S. R. Friberg and P. W. Smith, "Nonlinear Optical-Glasses for Ultrafast Optical Switches," *IEEE J. Quantum Electron.* **23** (12), 2089-2094 (1987).
- 24 K. Kikuchi, K. Taira, and N. Sugimoto, "Highly nonlinear bismuth oxide-based glass fibres for all-optical signal processing," *Electron. Lett.* **38** (4), 166-167 (2002).
- 25 D. W. Hall, M. A. Newhouse, N. F. Borrelli et al., "Nonlinear Optical Susceptibilities of High-Index Glasses," *Appl. Phys. Lett.* **54** (14), 1293-1295 (1989).
- 26 Xian Feng, T. M. Monro, V. Finazzi et al., "Extruded singlemode, high-nonlinearity, tellurite glass holey fiber," *Electron. Lett.* **41** (15), 835-837 (2005).
- 27 J. Requejo-Isidro, A. K. Mairaj, V. Pruneri et al., "Self refractive non-linearities in chalcogenide based glasses," *J. Non-Cryst. Solids* **317** (3), 241-246 (2003).
- 28 G.P. Agrawal, *Nonlinear Fiber Optics*, 2nd ed. (Academic Press, San Diego, 1995).

- 29 G. Brambilla, F. Koizumi, V. Finazzi et al., "Supercontinuum generation in tapered bismuth silicate fibres," *Electron. Lett.* **41** (14), 795-797 (2005).
- 30 F. Lu, Y. J. Deng, and W. H. Knox, "Generation of broadband femtosecond visible pulses in dispersion-micromanaged holey fibers," *Opt. Lett.* **30** (12), 1566-1568 (2005).
- 31 H. Ebendorff-Heidepriem, P. Petropoulos, S. Asimakis et al., "Bismuth glass holey fibers with high nonlinearity," *Opt. Express* **12** (21), 5082-5087 (2004).
- 32 J. Y. Y. Leong, S. Asimakis, F. Poletti et al., *Towards zero dispersion highly nonlinear lead silicate glass holey fibres at 1550 nm by structured-element-stacking*, ECOC, 31st European Conference on Optical Communications, Post Deadline paper TH.4.4.5, Glasgow, UK, 2005.
- 33 L.B. Shaw, P.A. Thielen, F.H. Kung et al., *IR Supercontinuum Generation in As-Se Photonic Crystal Fiber*, Conference on Advanced Solid State Lasers (ASSL), Technical Digest, Paper TuC5, 2005.
- 34 P. Petropoulos, H. Ebendorff-Heidepriem, V. Finazzi et al., "Highly nonlinear and anomalously dispersive lead silicate glass holey fibers," *Opt. Express* **11** (26), 3568-3573 (2003).
- 35 T. M. Monro, D. J. Richardson, N. G. R. Broderick et al., "Holey optical fibers: An efficient modal model," *J. Lightwave Technol.* **17** (6), 1093-1102 (1999).
- 36 T. M. Monro, N. G. Broderick, and D. J. Richardson, in *Nanoscale Linear and Nonlinear Optics: International School on Quantum Electronics, Erice, Sicily, July 2000*, edited by M. Bertolotti, C.M. Bowden, and C. Silbilia (AIP, Melville, NY, 2000), pp. 123-128.
- 37 A. V. Husakou and J. Herrmann, "Supercontinuum generation in photonic crystal fibers made from highly nonlinear glasses," *Appl. Phys. B-Lasers Opt.* **77** (2-3), 227-234 (2003).
- 38 Anatoly Efimov, F. G. Omenetto, A. J. Taylor et al., *Generation of UV Light from Microstructured Fibers Pumped with Femtosecond 800nm Oscillator*, Conference on Lasers and Electro Optics, Longbeach, California, 2002.
- 39 A. Efimov, A. J. Taylor, F. G. Omenetto et al., "Nonlinear generation of very high-order UV modes in microstructured fibers," *Opt. Express* **11** (8), 910-918 (2003).
- 40 G. Q. Chang, T. B. Norris, and H. G. Winful, "Optimization of supercontinuum generation in photonic crystal fibers for pulse compression," *Opt. Lett.* **28** (7), 546-548 (2003).
- 41 S. Coen, A. H. L. Chau, R. Leonhardt et al., "Supercontinuum generation by stimulated Raman scattering and parametric four-wave mixing in photonic crystal fibers," *J. Opt. Soc. Am. B-Opt. Phys.* **19** (4), 753-764 (2002).
- 42 M. H. Frosz, P. Falk, and O. Bang, "The role of the second zero-dispersion wavelength in generation of supercontinua and bright-bright soliton-pairs across the zero-dispersion wavelength," *Opt. Express* **13** (16), 6181-6192 (2005).
- 43 R. H. Stolen, C. Lee, and R. K. Jain, "Development of the Stimulated Raman-Spectrum in Single-Mode Silica Fibers," *J. Opt. Soc. Am. B-Opt. Phys.* **1** (4), 652-657 (1984).
- 44 R. H. Stolen, J. P. Gordon, W. J. Tomlinson et al., "Raman Response Function of Silica-Core Fibers," *J. Opt. Soc. Am. B-Opt. Phys.* **6** (6), 1159-1166 (1989).
- 45 T. P. White, R. C. McPhedran, C. M. de Sterke et al., "Confinement losses in microstructured optical fibers," *Opt. Lett.* **26** (21), 1660-1662 (2001).
- 46 A. Ferrando, E. Silvestre, P. Andres et al., "Designing the properties of dispersion-flattened photonic crystal fibers," *Opt. Express* **9** (13), 687-697 (2001).